Fabrication tolerant and broadband polarization splitter and rotator based on a taper-etched directional coupler

Yule Xiong,[1,2,*] Dan-Xia Xu,[1] Jens H. Schmid,[1] Pavel Cheben,[1] Siegfried Janz,[1] and Winnie N. Ye[2]

[1]*Information and Communication Technologies, National Research Council Canada, 1200 Montreal Road, Ottawa, Ontario, K1A 0R6, Canada*

[2]*Department of Electronics, Carleton University, 1125 Colonel By Drive, Ottawa, Ontario, K1S 5B6, Canada*

[*]*yxiong1@doe.carleton.ca*

Abstract: We propose a fabrication tolerant polarization splitter and rotator (PSR) on the silicon-on-insulator platform based on the mode-coupling mechanism. The PSR consists of a silicon wire waveguide coupled to a taper-etched waveguide. Compared to previously reported PSRs based on directional couplers which are sensitive to fabrication variations, the partially etched taper structure can compensate for fabrication inaccuracies. In addition, the taper-etched geometry breaks both the horizontal and vertical symmetries of the waveguide, introducing an additional degree of design freedom to accommodate different upper cladding layers. The proposed PSR can be readily integrated in a planar waveguide circuit using e.g. SiO_2 cladding, making it compatible with typical metal back-end-of-line processes. Our simulation results show that the PSR has a low TM-to-TE polarization conversion loss of –0.09 dB in the C-band (or a conversion efficiency of 98%). A low TE-to-TE through insertion loss (–0.07 dB) and a very low polarization crosstalk (–30 dB) over a wide wavelength range exceeding 160 nm with a large fabrication tolerance (>50 nm) are numerically demonstrated.

OCIS codes: (130.0130) Integrated optics; (130.3120) Integrated optics devices; (130.5440) Polarization-selective devices.

References and links

1. D. Dai, L. Liu, S. Gao, D.-X. Xu, and S. He, "Polarization management for silicon photonic integrated circuits," Laser Photon. Rev. **7**(3), 303–328 (2013).
2. T. Barwicz, M. R. Watts, M. A. Popović, P. T. Rakich, L. Socci, F. X. Kärtner, E. P. Ippen, and H. I. Smith, "Polarization-transparent microphotonic devices in the strong confinement limit," Nat. Photonics **1**(1), 57–60 (2007).
3. P. Dong, C. Xie, L. Chen, L. L. Buhl, and Y.-K. Chen, "112-Gb/s monolithic PDM-QPSK modulator in silicon," Opt. Express **20**(26), B624–B629 (2012).
4. H. Zhang, S. Das, Y. Huang, C. Li, S. Chen, H. Zhou, M. Yu, P. Guo-Qiang Lo, and J. T. L. Thong, "Efficient and broadband polarization rotator using horizontal slot waveguide for silicon photonics," Appl. Phys. Lett. **101**(2), 021105 (2012).
5. D. Vermeulen, S. Member, S. Selvaraja, P. Verheyen, P. Absil, W. Bogaerts, D. Van Thourhout, and G. Roelkens, "Silicon-on-insulator polarization rotator based on a symmetry breaking silicon overlay," IEEE Photon. Technol. Lett. **24**(6), 482–484 (2012).
6. Y. Xiong, D.-X. Xu, J. Schmid, P. Cheben, S. Janz, and W. Ye, "Robust silicon waveguide polarization rotator with an amorphous silicon overlayer," IEEE Photonics J. **6**(2), 2200308 (2014).
7. L. Chen, C. R. Doerr, and Y.-K. Chen, "Compact polarization rotator on silicon for polarization-diversified circuits," Opt. Lett. **36**(4), 469–471 (2011).
8. A. V. Velasco, M. L. Calvo, P. Cheben, A. Ortega-Moñux, J. H. Schmid, C. A. Ramos, I. M. Fernandez, J. Lapointe, M. Vachon, S. Janz, and D.-X. Xu, "Ultracompact polarization converter with a dual subwavelength trench built in a silicon-on-insulator waveguide," Opt. Lett. **37**(3), 365–367 (2012).
9. L. Liu, Y. Ding, K. Yvind, and J. M. Hvam, "Silicon-on-insulator polarization splitting and rotating device for polarization diversity circuits," Opt. Express **19**(13), 12646–12651 (2011).

#212815 - $15.00 USD Received 26 May 2014; revised 29 Jun 2014; accepted 30 Jun 2014; published 10 Jul 2014

10. Y. Ding, L. Liu, C. Peucheret, and H. Ou, "Fabrication tolerant polarization splitter and rotator based on a tapered directional coupler," Opt. Express **20**(18), 20021–20027 (2012).
11. H. Guan, A. Novack, M. Streshinsky, R. Shi, Q. Fang, A. E.-J. Lim, G.-Q. Lo, T. Baehr-Jones, and M. Hochberg, "CMOS-compatible highly efficient polarization splitter and rotator based on a double-etched directional coupler," Opt. Express **22**(3), 2489–2496 (2014).
12. J. Wang, B. Niu, Z. Sheng, A. Wu, X. Wang, S. Zou, M. Qi, and F. Gan, "Design of a SiO_2 top-cladding and compact polarization splitter-rotator based on a rib directional coupler," Opt. Express **22**(4), 4137–4143 (2014).
13. D. Taillaert, F. Van Laere, M. Ayre, W. Bogaerts, D. Van Thourhout, P. Bienstman, and R. Baets, "Grating couplers for coupling between optical fibers and nanophotonic waveguides," Jpn. J. Appl. Phys. **45**(8A), 6071–6077 (2006).

1. Introduction

Polarization management is an important topic of research in silicon photonic circuits [1]. Polarization splitters and rotators are structures of fundamental importance in polarization diversity systems [2] and polarization division multiplexed devices [3]. Various types of passive polarization splitters and rotators have been reported [4–12]. Mode-evolution polarization rotators [4–8] have attracted significant attention because of their broad operation wavelength range and robust fabrication tolerance, typically with amorphous silicon or silicon nitride overlayers used to modify the waveguide cross-section in order to break the waveguide vertical symmetry [4–7]. However, such devices generally require a rather complex fabrication process. Another class of polarization rotators are mode-coupling structures, which are inherently wavelength dependent and comparatively sensitive to fabrication variations. Polarization splitter and rotators (PSRs) using asymmetrical directional couplers (DCs) optimized for a single etch process have been reported [9, 10]. However, the air cladding is used to realize vertical asymmetry, which is incompatible with most metal back-end-of-line processes, and these devices are also sensitive to fabrication variations. Recently, double-etch asymmetrical wire and rib DC-based PSRs using silica cladding have been demonstrated [11,12]. The main practical issue of limited fabrication tolerance (typically <10 nm for a loss penalty of −1 dB) still remains.

Here we propose a fabrication tolerant and broadband PSR based on the mode-coupling mechanism. The PSR comprises a taper-etched DC, specifically a silicon wire waveguide evanescently coupled to a taper-etched waveguide. This design is compatible with silica upper cladding. The proposed PSR utilizes a partial etch process, which is available in most silicon photonics foundries.

2. Polarization splitter and rotator design

The proposed PSR is schematically illustrated in Fig. 1(a). It comprises a silicon wire waveguide (waveguide A) of width W and height H, coupled to a taper-etched waveguide (waveguide B) with a width W_t, a ridge width W_e, a post-etch slab height H_e, a taper angle θ, and a gap between the waveguides D_{gap}. The coupling length L_{DC} is the taper end-to-end distance in the waveguide B, where $L_{DC} = W_t/\tan(\theta)$. Two S-bends with a bending radius of R_S are used near the input and the output ports to decouple the waveguides in these two regions.

The operation principle of the PSR is as follows: The dimensions of the waveguide B are chosen based on two conditions: 1) a significant effective index mismatch of the TE-like mode (with dominant E_x component) for the waveguides A and B, i.e. $n_{eff}^{B}(TE) < n_{eff}^{A}(TE)$, to ensure that the TE-like mode injected in the input port A_1 propagates to the through port A_2 with a minimal cross-coupling to the waveguide B; 2) a phase matching condition $n_{eff}^{B}(TE) \sim n_{eff}^{A}(TM)$, so that the TM-like mode (with dominant E_y component) injected into port A_1 couples to the TE-like mode of the waveguide B. The coupling process from the TM-like mode in the waveguide A to the TE-like mode in the waveguide B is facilitated by hybrid modes supported in the waveguide B, in which both the horizontal and vertical asymmetries are created by the tapered-etch. Under these conditions, a high polarization conversion efficiency $CE_{TM\text{-}TE} = 10\log_{10}(P(out)^{B}_{TE}/P(in)^{A}_{TM})$ can be achieved.

#212815 - $15.00 USD Received 26 May 2014; revised 29 Jun 2014; accepted 30 Jun 2014; published 10 Jul 2014

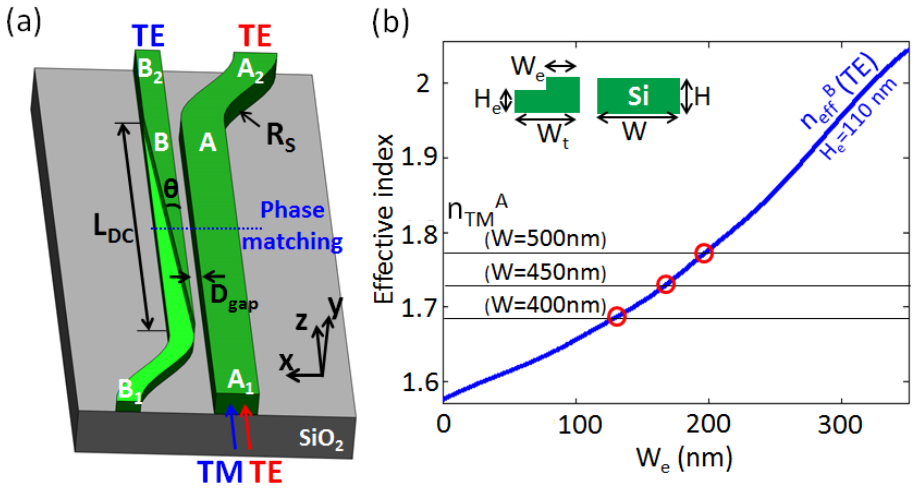

Fig. 1. (a) Schematic of the polarization splitter and rotator based on the taper-etched directional coupler. For clarity, the SiO_2 upper cladding is not shown. (b) Effective index of the TE-like mode of the taper-etched waveguide B as a function of the ridge width W_e for a post-etch height H_e = 110 nm, W_t = 350 nm, and H = 220 nm. Effective indices of the TM-like mode of the access waveguide A (H = 220 nm) are shown for different widths W of the access waveguide A (black lines). Red circles indicate the phase matching condition.

In our simulations we assume a free-space wavelength of 1550 nm, the refractive index of silicon n_{Si} = 3.476, the bending radius of S-bend R_S = 50 μm, and the upper and lower SiO_2 cladding with a refractive index n_{SiO2} = 1.444. The silicon layer thickness is H = 220nm, the width of the waveguide A is W = 450 nm, and the gap in the coupling section is D_{gap} = 200 nm, which are typical feature sizes used in silicon photonics foundries with public access. The robustness advantage of the proposed PSR can be observed in Fig. 1(b), which shows the TE-like mode effective index in the waveguide B as a function of its ridge width W_e for a post-etch slab height H_e = 110 nm. The TM-like mode effective indices of the waveguide A, n_{eff}^{A}(TM), are shown for three different waveguide widths. The TE-TM polarization coupling is achieved for the phase matching condition n_{eff}^{B}(TE) = n_{eff}^{A}(TM). This condition can be fulfilled for a specific combinations of parameters H_e, W_e and W_t of the coupling section. As the width of the waveguide A varies, the phase matching is still achieved just for a different W_e, i.e. at a different position along the taper. Similar behavior is also found for varying the post-etch slab height H_e. As a result, the TM-TE phase matching condition is remarkably insensitive to variations in waveguide dimensions.

The polarization conversion is further illustrated in Fig. 2, which includes the top views [Figs. 2(a) and 2(b)] and the cross-sectional views [Fig. 2(c)] of the mode evolution along the PSR structure, as calculated by the 3D-FDTD method. The TE-like mode launched in the input port A_1 propagates to the through port A_2 without cross-coupling [Fig. 2(a)]. On the other hand, the TM-like mode from the input port A_1 is gradually coupled to the waveguide B, being transformed into the TE-like mode propagating to the cross port B_2 [Fig. 2(b)]. Figure 2(c) shows the cross-sectional views of the mode evolution for the TM-like mode input. In the middle of the taper section, the E_x and E_y components are equalized, yielding an efficient mode hybridization.

In the following we optimize the device design by varying several parameters of the structure. We use the full-vectorial eigenmode expansion (EME) method and some results are cross-checked by the 3D-FDTD simulations.

#212815 - $15.00 USD Received 26 May 2014; revised 29 Jun 2014; accepted 30 Jun 2014; published 10 Jul 2014

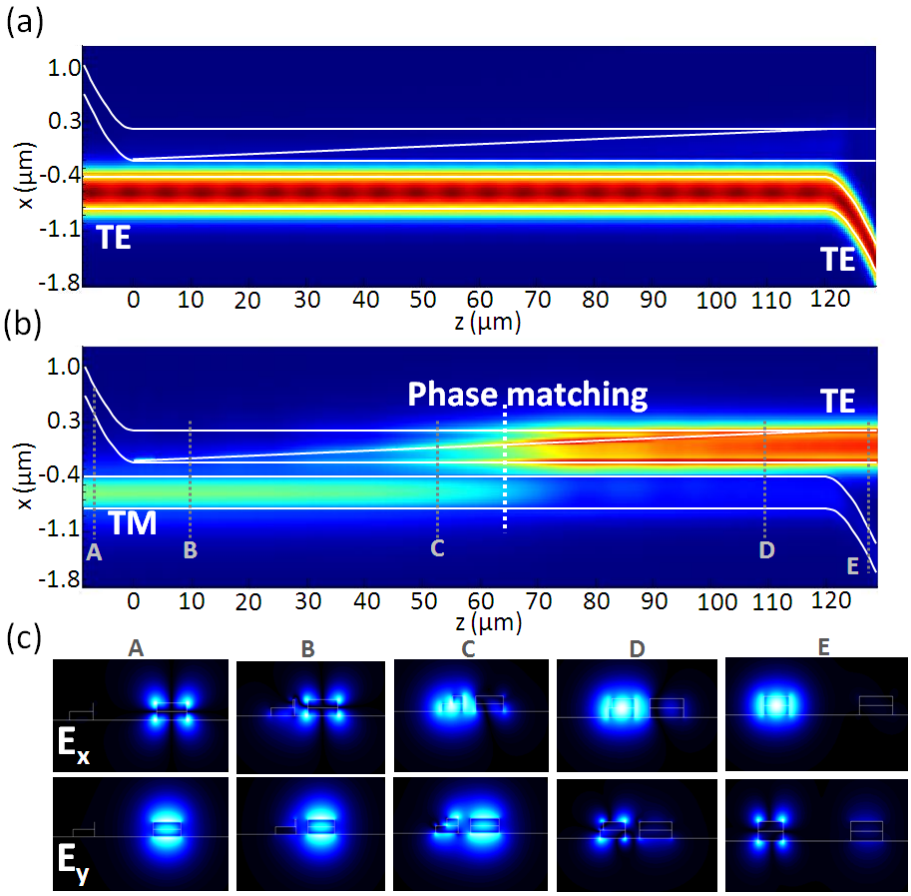

Fig. 2. Light intensity (Light input from the left port) of (a) TE-like mode input and (b) TM-like mode input evolution along the polarization splitter and rotator (top views), as calculated by a 3D-FDTD method. (c) Transverse electric field distributions at the corresponding positions along the polarization splitter and rotator when launching TM-like mode as input.

The PSR performance is examined for three post-etch slab heights: (i) H_e = 70 nm (deep etch with an etch depth of D = 150 nm); (ii) H_e = 110 nm (moderate etch depth, D = 110 nm); and (iii) H_e = 150 nm (shallow etch depth, D = 70 nm). The selection of these parameters is guided by the availability in foundry offerings. Figure 3(a) shows the effective indices of the TE-like mode in the waveguide B for these etch depths, as a function of the width ratio W_e/W_t. A deep etch introduces a large n_{eff}^B(TE) change in the coupling region and a longer coupling length L_{DC} is required [Fig. 3(b)].

The width W_t of the waveguide B should be sufficiently smaller than the width W of the waveguide A to avoid the TE-to-TE mode coupling between the two waveguides. Here, the phase matching condition is designed to be fulfilled in the middle of the taper section, i.e. n_{eff}^B(TE) = n_{eff}^A(TM) when $W_e = W_t/2$. By setting the width of the waveguide A to W = 450 nm, we obtain W_t = 410 nm, 350 nm and 310 nm for H_e = 70 nm, 110 nm, and 150 nm, respectively. These parameters are summarized in Table 1.

Using the selected values of parameters H_e and W_t, the polarization conversion efficiency CE_{TM-TE} is calculated as a function of the coupling length L_{DC} using the EME method. The results are shown in Fig. 3(b). For each etch depth, the polarization conversion efficiency eventually saturates and reaches its maximum value provided the coupler is long enough. For the shallow etch (H_e = 150 nm), a comparatively short L_{DC} is required. The L_{DC} values required for reaching the maximum polarization conversion efficiency CE_{TM-TE} are listed in Table 1. It is observed that the minimum polarization conversion loss (i.e., maximum CE_{TM-}

#212815 - $15.00 USD Received 26 May 2014; revised 29 Jun 2014; accepted 30 Jun 2014; published 10 Jul 2014

$_{TE}$) is achieved for a post-etch slab height of H_e = 110 nm. At this height (H_e = 0.5H), the mode is efficiently hybridized (50% E_x and 50% E_y) near the phase-matching position, yielding a high polarization conversion efficiency. Some of our results have been also verified using the 3D-FDTD method. For example, using the parameters in Table 1 for H_e = 110 nm, the calculated polarization conversion efficiency $CE_{TM\text{-}TE}$ is ~-0.09 dB across the entire C-band (from 1530 nm to 1565 nm), which is slightly better than the result obtained using the EME method.

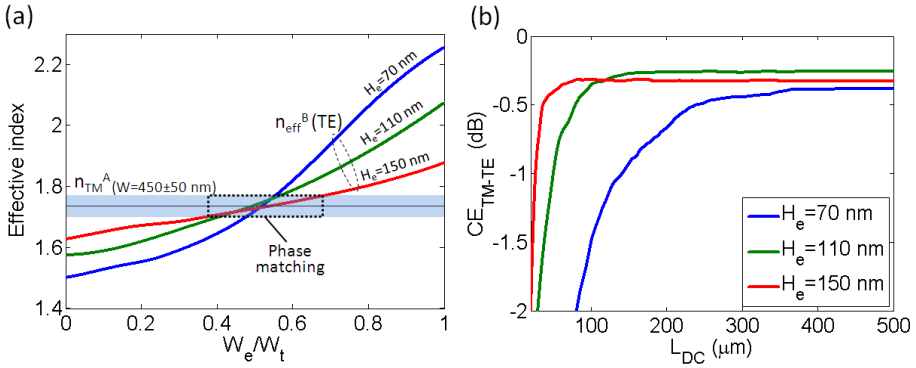

Fig. 3. (a) Effective index of the TE-like mode of the taper-etched waveguide B as a function of a width ratio W_e/W_t, for three different post-etch slab heights (H_e = 70 nm, 110 nm and 150 nm). The corresponding width W_t is 410 nm, 350 nm and 310 nm, for the phase matching near the position W_e/W_t = 0.5. Effective index of the TM-like mode of the access waveguide A (H = 220 nm) are shown for a waveguide width range W = 450 ± 50 nm (shadow region). (b) Polarization conversion efficiency $CE_{TM\text{-}TE}$ as a function of coupling length L_{DC} for post-etch slab heights H_e = 70 nm, 110 nm, and 150 nm.

Table 1. Optimized parameters of the polarization splitter and rotator calculated using the EME method

W (nm)	H (nm)	H_e (nm)	W_t (nm)	D_{gap} (nm)	L_{DC} (μm)	$CE_{TM\text{-}TE}$ (dB)
450	220	70	410	200	>390	–0.38
450	220	110	350	200	>120	–0.26
450	220	150	310	200	>80	–0.32

3. Fabrication tolerances

The designed taper-etched DC structures can be readily fabricated using the standard silicon photonics processing, including the two-step etch process often used for making high-efficiency surface grating couplers [13]. To investigate the fabrication tolerance of our PSR design, we study the polarization conversion efficiency $CE_{TM\text{-}TE}$ as a function of several device parameters, as shown in Fig. 4 and Table 2. Simulations show that the longer the coupling length L_{DC}, the more fabrication tolerant the PSR is, but with a penalty in device footprint. The reason is that a long coupling length L_{DC} provides a sufficiently long phase-matching region to ensure the full power transfer from the TM-like mode to the TE-like mode. Here, we set L_{DC} = 400 μm, 200 μm and 150 μm for H_e = 70 nm, 110 nm and 150 nm, respectively, larger than the values indicated in Table 1. Longer L_{DC} will slightly increase the insertion loss of the PSR while shorter L_{DC} decreases the fabrication tolerances. Figure 4(a) illustrates the dependence of polarization conversion efficiency $CE_{TM\text{-}TE}$ on the variation of the post-etch slab height (ΔH_e). All other parameters are assumed constant at their nominal design values listed in Table 1. It is observed that $CE_{TM\text{-}TE}$ is rather tolerant to over-etching (ΔH_e<0) in the taper section. On the other hand, $CE_{TM\text{-}TE}$ drops dramatically for substantial under-etching errors as the n_{eff}^A(TM) exceeds the maximum effective index range for which the phase matching condition holds.

#212815 - $15.00 USD Received 26 May 2014; revised 29 Jun 2014; accepted 30 Jun 2014; published 10 Jul 2014

Table 2. Calculated tolerances of the polarization splitter and rotator for CE_{TM-TE}> –0.5 dB and a TM-like input mode.

W (nm)	H (nm)	H_e (nm)	W_t (nm)	D_{gap} (nm)	D_t (nm)
450 ± 70	220 ± 30	70 + 40/-15	410 ± 25	200 ± 60	< 100
450 ± 55	220 ± 30	110 ± 25	350 ± 30	200 ± 100	< 95
450 ± 50	220 ± 28	150 + 18/-40	310 ± 25	200 ± 90	< 80

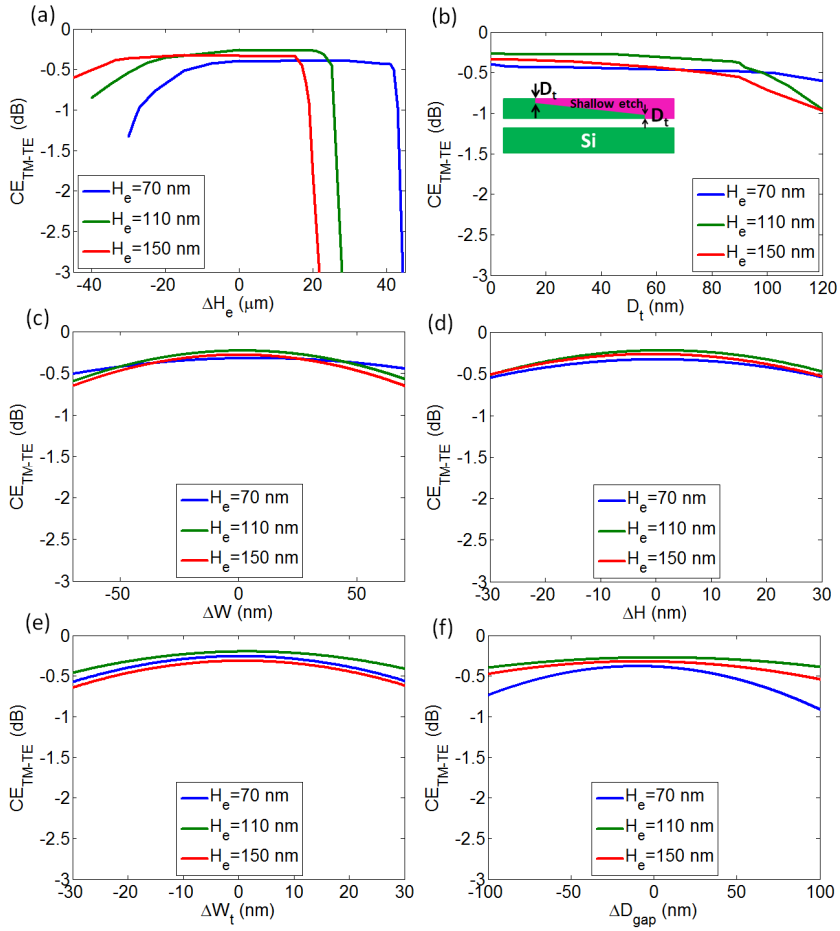

Fig. 4. Dependence of the polarization conversion efficiency CE_{TM-TE} on structure geometrical variations, calculated using the full-vectorial EME simulations for (a) post-etch slab height, ΔH_e, (b) tip width D_t, (c) width ΔW of the wire waveguide, (d) height ΔH of the wire waveguide, (e) width ΔW_t of the taper-etched waveguide, and (f) coupling gap ΔD_{gap}. The optimized parameters are listed in Table 1.

The fabrication tolerance of the PSR is also evaluated for other device parameters, with a condition of CE_{TM-TE}> −0.5 dB. For each scan of a given parameter, all other parameters are assumed constant at their nominal design values listed in Table 1. In practical implementation, the tip termination of the taper-etched waveguide has a finite width. Figure 4(b) shows the calculated polarization conversion efficiency CE_{TM-TE} as a function of tip with D_t. When D_t ~80 nm, CE_{TM-TE} is > –0.5 dB while the loss penalty is 0.2 dB. As shown in Table 2 and Fig. 4, the designed device is very fabrication tolerant to W, D_{gap} and D_t. Meanwhile, the fabrication tolerance of the proposed design is similar for different etching depths, i.e., H_e = 70 nm, 110 nm and 150 nm. In Table 2, it is also shown that the overall tolerances are better than 50 nm for a penalty of –0.5 dB in CE_{TM-TE}. These tolerances are

#212815 - $15.00 USD Received 26 May 2014; revised 29 Jun 2014; accepted 30 Jun 2014; published 10 Jul 2014

within the process specifications offered by photonic foundries, demonstrating the fabrication resilience of our PSR design.

Finally, we examine the operational wavelength range of our PSR. For a TE-like mode input, the TE-to-TE insertion loss (IL) at the through port A_2 and the crosstalk (XT) at the cross port B_2 are defined as $IL = 10\log_{10}(P(out)^{A}_{TE}/ P(in)^{A}_{TE})$ and $XT_{TE} = 10\log_{10}(P(out)^{B}_{TE} /P(out)^{A}_{TE})$ respectively. For the TM-like mode input, the polarization conversion loss (PCL) at the cross port B_2 and the XT at the through port A_2 are defined as $PCL = 10\log_{10}(P(out)^{B}_{TE}/ P(in)^{A}_{TM})$ and $XT_{TM} = 10\log_{10}(P(out)^{A}_{TE}/P(out)^{B}_{TE})$, respectively. Figure 5 shows the wavelength dependence of the loss and crosstalk of the PSR for H_e = 110 nm. The TE-like mode insertion loss is below −0.07 dB within the wavelength range of 1450 nm to 1650 nm (bandwidth>200 nm), while the TM-to-TE conversion loss is less than −0.5 dB across the entire S, C and L-bands (1460 nm to 1625 nm), and below −0.3 dB over the C-band (1530 nm to 1565 nm). As shown in Fig. 5(b), the crosstalk XT_{TE} and XT_{TM} are below −30 dB in the investigated S, C and L bands. This broad bandwidth is a distinct advantage of our PRS based on the taper-etched directional coupler. In Table 3 we summarize the wavelength dependence of the PSR parameters for the three different post-etch slab heights H_e. For the deep-etch (H_e = 70 nm), the TE-to-TE insertion loss is about −0.15 dB and the crosstalk XT_{TM} is below −20 dB. This is because the width W_t = 410 nm of the waveguide B is closer to W = 450nm, resulting in TE-to-TE mode coupling between the two waveguides. In addition, simulations show that fabrication tolerances remain similar over the entire C band. Since n_{eff}^{B}(TE) of the waveguide B and n_{eff}^{A}(TM) of the waveguide A varies with the wavelength in a similar trend, the phase-matching condition $n_{eff}^{B}(TE) = n_{eff}^{A}(TM)$ is expected to be achieved at the same position for different wavelengths.

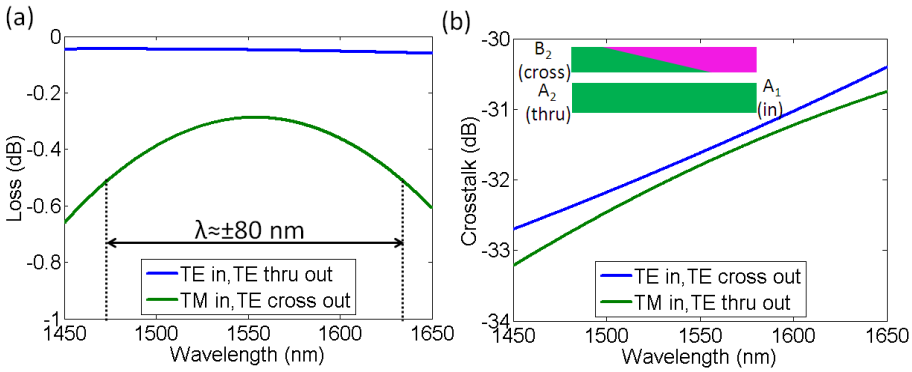

Fig. 5. Wavelength dependence of the polarization splitter and rotator as calculated by the full-vectorial EME simulations. (a) TE-like mode insertion loss and TM-to-TE polarization conversion loss; (b) Crosstalk XT_{TE} and XT_{TM}. W = 450 nm, H = 220 nm, W_t = 350 nm, H_e = 110 nm, D_{gap} = 200 nm, and L_{DC} = 200 μm.

Table 3. Performance of the polarization splitter and rotator for the S, C and L bands (the wavelength range from 1460 nm to 1625 nm)

H_e (nm)	W_t (nm)	IL (dB)	XT_{TE} (dB)	PCL (dB)	XT_{TM} (dB)
70	410	>-0.15	<-25	>-0.5	<-15
110	350	>-0.07	<-30	>-0.5	<-30
150	310	>-0.05	<-30	>-0.5	<-30

4. Comparison with literature results

Table 4 summarizes several results of the DC-based PSRs from the current literature and compares them with our design. The PSRs using a one-step etch in [9, 10] required an air cladding to break the vertical asymmetry in order to achieve a high polarization conversion efficiency. The two-step etching processes in [11, 12] induced both the horizontal and vertical asymmetry without the need of an air cladding. However, the parallel DC structures in [9, 11,

#212815 - $15.00 USD Received 26 May 2014; revised 29 Jun 2014; accepted 30 Jun 2014; published 10 Jul 2014

12] required precisely tuned phase matching. As a result, these DCs are all inherently wavelength dependent and sensitive to fabrication variations. The tapered DC in [10] was used to compensate the fabrication variations at the cost of a relatively large footprint. However, the improvement of the fabrication tolerance was still limited. The taper-etched DC structure in this work enhances the fabrication tolerance significantly while using a similar footprint as in [10]. Furthermore, the structure reported here has a broadband operation bandwidth without the need for precise lithographic alignments.

Table 4. Comparison of directional coupler based polarization splitter and rotator.

Reference	Height (nm)	Gap (nm)	Length (μm)	Cladding	Tolerance (nm)	Bandwidth (nm)
[9]	250	100	36.8	air	<10	35 (C band)
[10]	250	100	>100	air	14	35 (C band)
	250	150	>200	air	14	35 (C band)
[11]	220	150	27	SiO_2	<10	30
[12]	250	150	24	SiO_2	<10	100
Our work	220	200	>80	SiO_2	50*	160

*Note the fabrication tolerances for Refs [9–12]. refer to a criterion of CE_{TM-TE}>-1 dB, while for the current work the criterion is for CE_{TM-TE}>-0.5 dB.

5. Conclusion

We have proposed and investigated a fabrication-tolerant polarization splitter and rotator (PSR) design based on the cross-polarization coupling mechanism. The PSR comprises a silicon wire waveguide coupled to a taper-etched waveguide and it can be fabricated by standard silicon photonics processing without the need for precise lithographic alignments. We used the full-vectorial EME and the 3-D FDTD methods for the numerical evaluation of the device performance. Our calculations show that a high TM-to-TE polarization conversion efficiency can be readily achieved over a broad wavelength range, i.e. −0.5 dB polarization conversion loss within the S, C and L band wavelength range of exceeding 160 nm. The conversion loss in the C-band is below −0.09 dB. A TE-to-TE through insertion loss is better than −0.07 dB for the same wavelength range, with a low polarization crosstalk of −30 dB. Among the PSR structures designed for an SOI platform, our design is among the most fabrication tolerant and broadband reported to date.

#212815 - $15.00 USD Received 26 May 2014; revised 29 Jun 2014; accepted 30 Jun 2014; published 10 Jul 2014